Modeling the RNA 2'OH activation: possible roles of metal ion and nucleobase as catalysts in self-cleaving ribozymes

Zdeněk Chval, Daniela Chvalová, Fabrice Leclerc

THE JOURNAL OF PHYSICAL CHEMISTRY B

ARTICLE

pubs.acs.org/JPCB

Modeling the RNA 2′OH Activation: Possible Roles of Metal Ion and Nucleobase as Catalysts in Self-Cleaving Ribozymes

Zdeněk Chval,*[,†,§] Daniela Chvalová,[‡] and Fabrice Leclerc*[,§]

[†]Department of Laboratory Methods and Information Systems, Faculty of Health and Social Studies, University of South Bohemia, J. Boreckého 27, 370 11 České Budějovice, Czech Republic

[‡]Department of Applied Chemistry, Faculty of Agriculture, University of South Bohemia, Branišovská 31, 370 05, České Budějovice, Czech Republic

[§]Laboratoire ARN, RNP, structure-fonction-maturation, Enzymologie Moléculaire et Structurale (AREMS), UMR 7214 CNRS-UHP Nancy 1, Faculté des Sciences et Technologies, B.P. 70239, 54506 Vandoeuvre-lès-Nancy, France

Supporting Information

ABSTRACT: The RNA 2′OH activation as taking place in the first chemical step of self-cleaving ribozymes is studied theoretically by DFT and MP2 methods using a continuum solvation model (CPCM). The reaction of proton transfer is studied in the presence of two kinds of catalysts: a fully hydrated metal ion (Mg^{2+}) or partially hydrated nucleobase (guanine), taken separately or together leading to three different modes of activation. The metal ion is either directly bound (inner-sphere) or indirectly bound (outer-sphere) to the 2′OH group and a hydroxide ion acts as a general or specific base; the nucleobase is taken in anionic or in neutral enol-tautomeric forms playing itself the role of general base. The presence of a close metal ion (outer-sphere) lowers the pK_a value of the 2′OH group by several log units in both metal-ion and metal-ion and nuleobase catalysis. The direct metal coordination to the 2′OH group (inner-sphere) further stabilizes the developing negative charge on the nucleophile. The switching from the inner-sphere to the outer-sphere coordination appears to be driven by the energy cost for reorganizing the first coordination shell rather than by the electrostatic repulsion between the ligands. The metal-ion catalysis is more effective with a specific base in the dianionic mechanism. On the other hand, the nucleobase catalysis is more effective in the monoanionic mechanism and in the presence of a metal ion acting as a cofactor through nonspecific electrostatic interactions. The results establish a baseline to study the possible roles of metal and nucleobase catalysts and their environment in more realistic models for self-cleaving ribozymes.

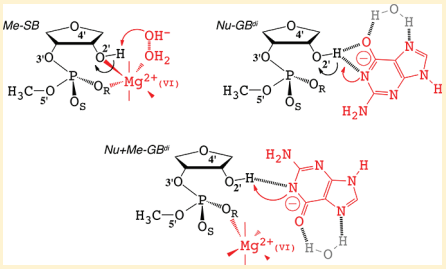

INTRODUCTION

Natural RNA enzymes catalyze phosphodiester autocleavage reactions to give products with 5′-hydroxyl and 2′-3′-cyclic phosphate termini or 5′-phosphate and 3′-hydroxyl termini: a chemical signature from self-cleaving or self-splicing ribozymes, respectively. In both types of ribozymes, the cleavage reaction proceeds through a S_N2-type in-line attack mechanism with an inversion of the stereochemical configuration of the nonbridging oxygen atoms about the scissile phosphorus atom. The S_N2-type in-line mechanism involves a trigonal bipyramidal transition state that is formed after the nucleophilic attack (once the nucleophile is activated) on the phosphorus and before the departure of the leaving group. From the data accumulated on several ribozymes, it was suggested in review articles that self-cleaving and self-splicing ribozymes employ distinct catalytic strategies that rely on metal ions or nucleobases as catalysts, respectively.[1−3] The active site of self-splicing ribozymes has a higher charge density because of the presence of an additional exogenous or endogenous nucleotide cofactor (a guanosine in group-I introns or an adenosine in group-II introns). It might explain the requirement for divalent metal ions in a catalytic strategy based on a two-metal-ion mechanism in group I[4] or group II self-splicing introns.[1] In self-cleaving ribozymes, the role of nucleobases as catalysts has been generalized, although they may intervene in very different ways[3] including in a cooperative way with metal ions.[5]

The two major steps of the reaction are (1) the phosphoryl transfer resulting from the nucleophilic attack and (2) the proton transfer to the 5′-oxygen leaving group. Not only the departure of the leaving group but also the nucleophilic attack involve some acid/base catalysis. A proton transfer is involved both in facilitating the departure of the leaving group and in activating the attacking nucleophile (Figure 1). In the nonenzymatic reaction, the catalysis may proceed by a specific acid/base catalysis (dianionic mechanism) or a general acid/base catalysis (monoanionic mechanism) where one of the phosphate oxygens can operate as an internal base (Figure 1A). In the enzymatic reactions, the nucleophile is either an internal 2′-hydroxyl in self-cleaving ribozymes or an external hydroxyl in self-splicing ribozymes that can be a 3′-hydroxyl (group I introns) or a 2′-hydroxyl (group II introns).

Received: January 29, 2011
Revised: August 6, 2011

dx.doi.org/10.1021/jp200970d | J. Phys. Chem. B XXXX, XXX, 000–000

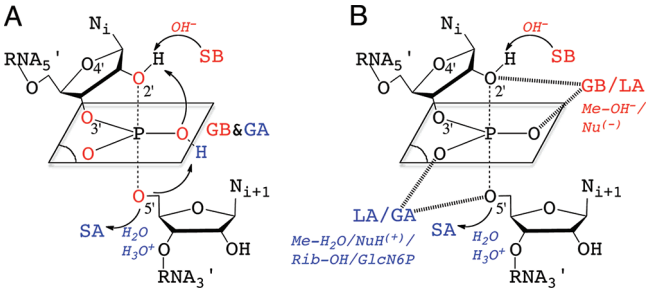

Figure 1. Acid/base activations of the 5′-oxygen leaving group and 2′-oxygen nucleophile in the catalysis by self-cleaving ribozymes: (A) nonenzymatic reaction; (B) enzymatic reaction. Abbreviations: SB, specific base; GB, general base; GA, general acid; SA, specific acid; Rib, ribose; Nu, nucleobase; Me: metal.

Table 1. Activation Modes of the Nucleophile and Leaving Group Associated with Proton Transfers[a]

ribozyme	2′-hydroxyl deprotonation	5′-oxygen protonation
hammerhead	Nu-GB($G12^-$)[34]	Me-GA/Rib2′OH-GA-(Mg^{2+}/H_2O& G8-OH)[20]
	Me-GB(Mg^{2+}/OH^-)[11,13,15]	
	Me-SB(Mg^{2+}&OH^-)[55]	
hairpin	Nu-GB($G8^-$)[56−58]	Nu-GA($A38H^+$)[56−58]
	Nu-SB(G8&OH^-)[16,59,60]	Nu-SA(A38& H_2O)[16,59,60]
HDV	Nu-GB(C75)[22,61]	Me-GA(Mg^{2+}/H_2O)[22,61]
		Me-SA(Mg^{2+}/H_2O)
	Me-GB(Mg^{2+}/OH^-)[21,62−64]	Nu-GA($C75H^+$)[21,62−64]
	Me-SB(Mg^{2+}/OH^-)[64]	
VS	Nu-GB($G638^-$/A756)[65,66]	Nu-GA(A756)[65,66]
glmS	Nu-GB(G33)[37,67]	Glc*-GA(GlcN6PH$^+$)[37,67]

[a] Me: metal ion, Nu: nucleobase, Rib: ribose, GA: general acid, GB: general base, SA: specific acid, SB: specific base, Glc: glucosamine-6-phosphate.

A general or specific base catalyst can activate the nucleophile by removal of the proton from the hydroxyl group (Figure 1B). Similarly, a general or specific acid can facilitate the departure of the 5′-oxygen leaving group. Among the self-cleaving ribozymes studied (Hammerhead, Hairpin, HDV, VS, glmS), different catalytic strategies have been proposed.[2,6] Although these strategies may be reduced to four basic ways to promote the reaction,[7] there is still a large diversity of catalysts that may play similar roles depending on the organization and dynamics of the active site. We can classify the catalysts in different families, whether they act as general/specific acid or base and whether they are metal ion or nucleobase. As summarized in Table 1, all eight possible combinations are represented in the models proposed and are supported by some experimental data. However, metal ions are associated with either general or specific acid/base whereas nucleobases are more tightly combined as general acid or base. In the case of the hairpin and HDV ribozymes, the experimental data are consistent with either specific or general acid/base. In the hairpin ribozyme, nucleobases are the only catalysts. On the other hand, both metal ions and nucleobases are supported as catalysts in the HDV ribozyme. Opposite models were proposed depending on the roles assigned to the nucleobase (C75) and the metal ion (Mg^{2+}) as base and acid, respectively or vice versa.

The nucleophile activation through the 2′-hydroxyl deprotonation is generally considered as minor because the chemical process itself is not rate-determining in the overall reaction. Besides, the possible interference with induced conformational changes related to solvent effects or presence of divalent metal ions[8−10] makes it difficult to evaluate precisely the energetics of this step in the reaction mechanism. A first and simple approach is to study the elementary chemical processes associated with the nucleophile activation in solution, excluding the influence of the active site and its environment. Theoretical approaches are particularly appropriate to study the energetics of the reaction and provide a baseline for the evaluation of the contributions coming from the active site preorganization and reorganization. The extension of the study to the full ribozymes would then allow us to evaluate the influence of the active site and the catalytic efficiency resulting from their molecular evolution.

In the models proposed from theoretical calculations, different activation modes have been examined depending on the proposed reaction mechanism. All the activation modes were not fully or exhaustively explored (Figure 2). Most of the studies based on classical QM approaches systemically neglect the contributions from the metal binding to the ribose−phosphate moiety and the rearrangements associated with changes of metal coordinations occurring before the deprotonation (Figure 2A). They were also initially focused on minimalist models of self-cleaving (hammerhead) ribozymes and a general acid/base catalysis with metal ions as unique catalysts (Figure 2C).[11−15] Other activation modes using nucleobases as catalysts have been studied more recently using hybrid QM/MM approaches applied to the hairpin,[16,17] hammerhead,[18−20] and HDV[21,22] ribozymes (Figure 2B,F). The comparison of the results obtained using QM/MM or QM approaches, including (or not) the environment of the active site from the ribozyme structures, will be valuable to evaluate the influence of the active site reorganizations on the catalytic efficiency. However, the available data are currently too limited for such comparison. In the hammerhead ribozyme for example, the nucleophile activation is skipped in the QM/MM studies and the nucleophile is usually considered as already activated.[23]

Using DFT methods, the activation barriers for the nonenzymatic and uncatalyzed reaction of activation have been calculated by Boero et al.[12] and Lopez et al.[14] with a pretty good accordance giving a Gibbs free energy barrier for the nucleophile activation between 28 and 30 kcal/mol (depending on the sugar pucker) in the case of the GB^{mono} activation mode (Figure 1A). The presence of metal catalysts and their influence on the energy barrier has been studied using minimalist QM models in nonenzymatic reactions (Figure 2B,C).[11,13,15] The presence of a metal ion close to the 2′-oxygen contributes to lowering the energy barrier even more when the metal ion is directly coordinated (Me-GB^{mono}: Figure 2B).[12] Furthermore, the presence of a second noncatalyst metal ion, in the Me-GB^{mono} activation mode, has a cooperative effect.[13] A cooperative effect between a nucleobase and a metal ion effect was also suggested recently in the nucleophile activation of the hammerhead ribozyme,[5] but no QM study on such model has been done yet (example: Figure 2G). On the other hand, the activation barrier for the nucleophile activation by a nucleobase has been calculated for the hairpin ribozyme[16] but only for the monoanionic mechanism (Figure 2F).

In none of the self-cleaving ribozymes is the nucleophile activation the rate-limiting step, but the activation barrier may be underestimated when, for example, the energy barrier for

dx.doi.org/10.1021/jp200970d |J. Phys. Chem. B XXXX, XXX, 000–000

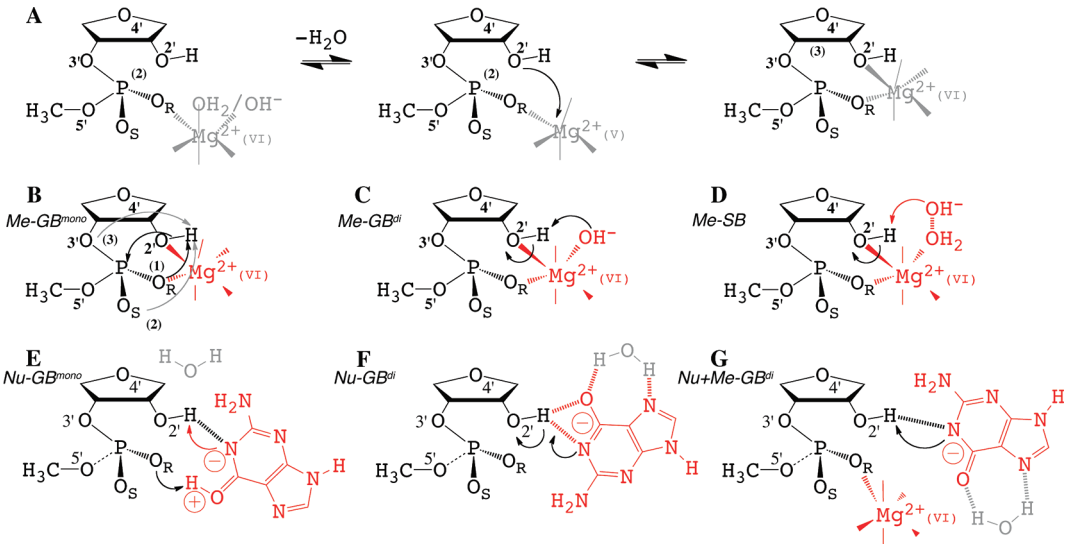

Figure 2. Activation modes of the 2′OH nucleophile. (A) Coordination change step by inner-sphere coordination to the 2′-oxygen. (B) Activation by a general base through an internal proton transfer (monoanionic mechanism). (C) Activation by a general base through a metal OH^- ligand (dianionic mechanism). (D) Activation by a specific base through a OH^- ligand. (E) Activation by a general base: a nucleobase in a tautomeric form (monoanionic mechanism). (F) Activation by a general base: a nucleobase in an ionized form (dianionic mechanism). (G) Activation by a general base: a nucleobase in an ionized form assisted by a metal.

going from a loosely bound to a tightly bound metal to the 2′OH (outer-sphere to inner-sphere coordination) in the Me-GB or Me-SB activation modes is neglected. Thus, one may misinterpret the comparison of role and influence of different catalysts when trying to predict the more favorable reaction mechanisms.

In the current study, we describe and analyze the reaction mechanisms for a selection of four different activation modes: Me-GB, Me-SB, Nu-GB, and Me+Nu-GB (Figure 2). The first three activation modes correspond to the more representative supported models in self-cleaving ribozymes, i.e., Me-GB, Me-SB and Nu-GB (Table 1); the last one corresponds to a new cooperative model between a metal ion and a nucleobase (Me+Nu-GB). In the case of Me-GB or Me-SB modes, the rearrangements necessary for metal coordination (preactivation) have also been taken into account. For the sake of comparison between mono- and dianionic mechanisms on the one hand and between general or specific base catalysis on the other hand, activation modes studied previously (Figure 2C,F) have been evaluated as well at the same level of theory. In the case of Me-GB^{mono}, both paths involving the proton transfer on either of the two nonbridging oxygens are well-known but in different contexts: the nonenzymatic and uncatalyzed reaction,[14] the nonenzymatic reaction in the presence of a metal ion as catalyst[13] (Figure 2B) or the enzymatic reaction in the hairpin ribozyme but using a nucleobase as catalyst.[24] This activation mode is evaluated in the presence of a metal ion as catalyst for three reactions paths: the two well-known reaction paths and a third alternative and new path where the proton is transferred to the bridging 3′-oxygen (Figure 2B). In the case of the activation by a nucleobase (Nu-GB), it has been previously studied in the context of the hairpin ribozyme[24] (Figure 2F) but the catalyst was a charged and thus activated nucleobase (Nu-GB^{di}); a neutral tautomeric form is considered here as well to evaluate the monoanionic mechanism of the activation reaction (Nu-GB^{mono}; Figure 2E). Finally, a cooperative model between a nucleobase and a metal ion is proposed and compared to the other activation modes. The following steps of the reaction are then considered to determine how the activation mode orients the reaction path for the nucleophilic attack and eventually the departure of the leaving group and how it impacts the energy barriers.

THEORETICAL METHODS AND ENERGY MODELS

High level ab initio calculations (DFT and MP2) were performed with the Gaussian 03 program package.[25] The Molden program[26] was employed to visualize the geometric and electronic features of the structures and XCrysden program[27] for final structure presentation. A 3′-phosphorylated ribose moiety is considered as a model system for the self-cleaving reaction. All structures were fully optimized using the B3LYP density functional theory method with 6-31+G(d) basis set. The nature of the obtained stationary points was always checked by a vibrational analysis. Thermal contributions to the energetic properties were calculated using canonical ensemble of statistical mechanics at standard conditions (T = 298 K, p = 101.325 kPa). Single point energy calculations on the optimized geometries were carried out with a more flexible 6-311+G(2d,2p) basis set.

The optimization on the B3LYP/6-31+G* level gives a Mg−O bond length of 2.109 Å for $[Mg(H_2O)_6]^{2+}$ that is in complete agreement with X-ray diffraction data (Mg−O = 2.11 Å).[28] However, when DFT and MP2 energies are compared, the latter show significantly stronger preference for hexacoordinated $Mg(H_2O)_6^{2+}$ ion with respect to pentacoordinated $Mg(H_2O)_5\cdot(H_2O)^{2+}$ ion.[29] Although the former ion is more stable than the latter by 2.2 kcal/mol on the B3LYP/6-311++G(d,p) level, the MP2(FULL)/6-311++G(d,p) method offers a much higher value of 6.2 kcal/mol.[29] Both numbers decrease with increasing basis set but the difference of about 3−4 kcal/mol remains (1.4 kcal/mol vs 4.6 kcal/mol for 6-311++(3df,3dp) basis set[29]). This trend was confirmed in our calculations, although we obtained slightly higher values, because we had to use a smaller basis set due to the size of our system. On the B3LYP/6-311+G(2d,2p)//6-31+G* level the $[Mg(H_2O)_6]^{2+}$ complex is by 2.5 kcal/mol more stable than the $[Mg(H_2O)_5]^{2+}(H_2O)$ complex.

dx.doi.org/10.1021/jp200970d |J. Phys. Chem. B XXXX, XXX, 000–000

The MP2(FC)/6-31+G**//B3LYP/6-31+G* scheme gives the difference of 6.5 kcal/mol. Because the 2′OH activation mechanism involves a Mg^{2+} coordination change step, MP2(FC)/6-31+G**//B3LYP/6-31+G* single point energies are also shown for a comparison in relevant cases. Relative free energies at the MP2 level clearly favor hexacoordinated Mg^{2+} structures; otherwise all trends of energy are consistent with DFT results.

To evaluate the solvent influence on the energetics of the reaction, single point calculations on the gas-phase optimized geometries were performed using CPCM continuum solvation model on the B3LYP/6-311+G(2d,2p) level of theory (the same level as the gas-phase single points). All solvent-phase calculations were carried out in water (ε_r = 78.39). Default CPCM parametrization as implemented in G03 was used. These calculations are denoted as DFT-CPCM in further text. The solvation corrections calculated by B3LYP were used also for MP2 energies. MP2 gas-phase energies combined with DFT solvation corrections are denoted as MP2-CPCM energies in further text. The electrostatic potential-fitted atomic charges were used to describe changes in electrostatic properties.

Additional single-point calculations on selected G03-optimized structures were conducted using the Amsterdam Density Functional 2001.01 package (ADF)[30] to calculate fragment energy decompositions according to the extended transition state theory.[31] In these calculations, a triple-ζ STO basis set is used, with one set of polarization functions as provided in the ADF, together with the BLYP functional.

Exact theoretical determination of pK_a values is still tricky, especially for charged metal complexes. Our estimations of pK_a values are based on the comparisons of relative energies using a standard expression $\Delta pK_a = -\Delta(\Delta G)/2.303RT$.

In the model compounds, the positions of the metal and the nucleobase, with respect to the ribose−phosphate moiety, were initially determined on the basis of X-ray data: the more favorable binding site for Mg^{2+} around phosphate groups[32,33] and the positions of the nucleobase in the catalytic pocket of a full-length hammerhead ribozyme.[34] Only the phospho-ribose moiety of the residue C17 and the nucleobase of the residue G8 base were extracted; the other atoms were not included (PDB ID: 2GOZ).[34]

STRUCTURE LABELING

In metal-based activation models (Me-GB and Me-SB) the structures are labeled by roman numbers starting from reactants to products in the progressive order along the reaction coordinate. The basic model system is neutral and consists of 3′-phosphorylated ribose (−1), a magnesium ion (+2) with four water and one OH^- (−1) ligands. The 3′-phosphorylated ribose is a monoanion that is converted into a dianion during the nucleophile activation (the dianionic mechanism). The structures are labeled by a roman number (from I to VII) and the symbol w. In a monoanionic mechanism, the structures have one more proton than those in the dianionic mechanism, so they are labeled by an additional H symbol. The coordination number of the Mg^{2+} ion can change during the reaction, expelling one water ligand to the second hydration shell. When this happens, those water molecules are not considered in the forward chemical steps along the reaction path (see below) and the corresponding structures are labeled without the w symbol.

Two structures with identical roman numbers are at an equivalent stage of the reaction. For example, the starting structures, labeled "I", correspond to the reactant with a hexacoordinated magnesium and the 2′OH group in the second coordination shell and the final structures, labeled "VII", correspond to the product of activation with the active 2′O^- group directly coordinated to magnesium. An Arabic number is added when necessary to distinguish different isomers of the same model compound.

In Me-GB models, the possible rate-determining transition states for the cleavage reaction were also optimized. They correspond to a final proton transfer to the 5′-oxygen of the leaving group and they are designated as "TSH-Ox" and "TS-Ox" for the transition states resulting from Me-GB^{mono} and Me-GB^{di} pathways, respectively. The letter "x" refers to a proton acceptor, and it can be replaced by "w", "R", "S", or "3" corresponding to the oxygen atom of a water molecule, a nonbridging oxygen from the phosphate group (pro-R_p, pro-S_p), or the bridging oxygen from the 3′OH group, respectively.

In the Nu-GB and Nu+Me-GB models the 2′OH group of the ribose moiety is activated by the guanine nucleobase. Here, the reactant (R), transition state (TS), and product (P) structures are designated as Nu-GB/R, Nu-GB/TS, and Nu-GB/P, respectively. In the Nu+Me-GB activation mode, two additional water molecules are present in the second coordination shell of the metal.

RESULTS

The activation modes are classified and examined depending on the catalyst (metal ion/nucleobase) and its role (general/specific base) and the reaction mechanism (dianionic/monoanionic), as shown in Figure 2. For both kinds of catalysts, the monoanionic and dianionic mechanisms are considered. The rearrangements related to changes in conformation and metal coordinations are taken into account as a preactivation step associated with the switch from an outer- to inner-sphere coordination that subsequently facilitates the activation by increasing the proton acidity (Figure 2A).

In the monoanionic mechanism, the 2′OH activation is coupled with the nucleophilic attack. In the uncatalyzed reaction, the proton is transferred to one of the nonbridging oxygens before the nucleophilic attack occurs[14,16] as the in-line conformation is adopted. In the catalyzed reaction, a similar reaction path has been proposed for the nucleobase catalysis (Nu-GB^{mono}) in the hairpin ribozyme.[16,24] The two chemical steps are concerted in the metal catalysis (Me-GB^{mono}) where the in-line attack and the proton transfer occur simultaneously via a late proton transfer.[13] Unfortunately, the energy barrier for the 2′OH activation and nucleophilic attack are not specified. In this study, we consider the monoanionic mechanism as proposed for the uncatalyzed and catalyzed reactions where the 2′OH activation and the nucleophilic attack are coupled but not concerted. Thus, we can provide precise data on the 2′OH activation for Me-GB^{mono} (Figure 2B) and compare with the available data in the presence of a nucleobase catalyst: Nu-GB^{mono}.[14,16]

In the dianionic mechanism, the 2′OH activation is supposed to be disconnected from the nucleophilic attack. We can still assume that the activation takes place either before or after some conformational rearrangement in the in-line attack for Nu-GB^{di} (Figure 2F) and Me-GB^{di} (Figure 2C), respectively. In the particular case of Me-GB^{di}, we may further distinguish two situations where the 2′-oxygen is within the first or second coordination sphere of the metal: both situations have been considered to determine the influence of the inner-sphere/outer-sphere coordinations on the 2′OH activation and the following steps of the reaction. The Me-SB activation mode follows a

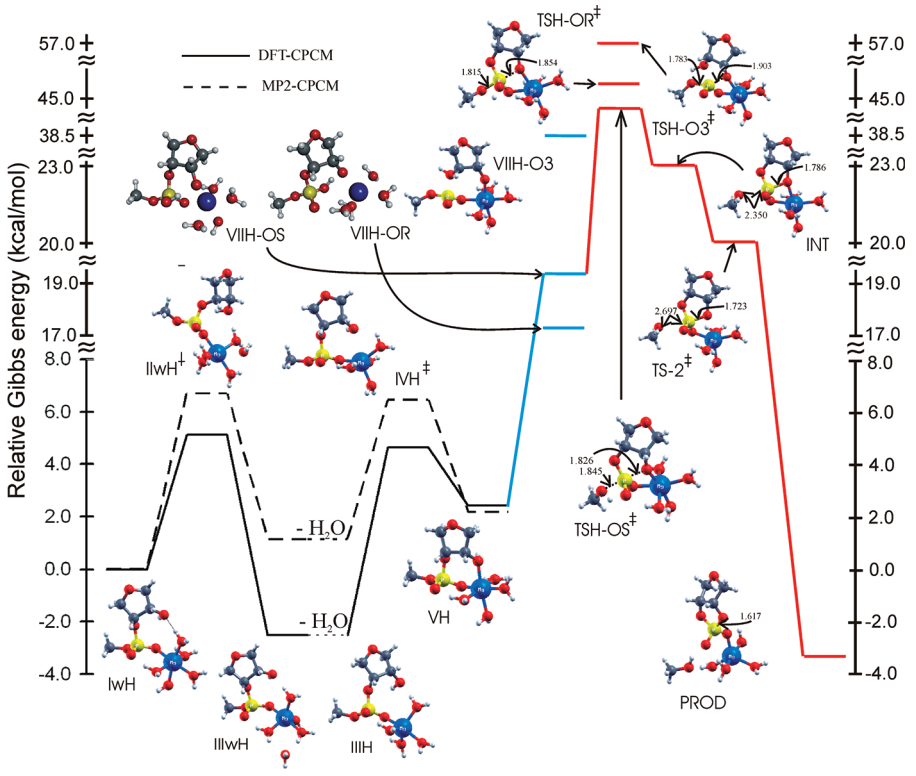

Figure 3. Gibbs free energy surface for the monoanionic pathway (Me-GB^{mono} activation modes). The black lines correspond to the preactivation step (structures from IwH to VH). The blue line corresponds to the 2′OH activation, and the red line corresponds to the final cleavage reaction. Structures VH-OR, VH-OS, VIH-OR‡, and VIH-OS‡ are omitted for the clarity. VH can be activated also by an external base (Figure 5). See the text for a more detailed description of the stationary points. Lines: full, DFT-CPCM pathway; dashed, MP2-CPCM pathway.

preactivation similar to the step in the monoanionic mechanism described here (Me-GB^{mono}) for switching from an outer-sphere to an inner-sphere coordination to the 2′-oxygen. Then, a specific base (OH^-) in the second coordination sphere abstracts the proton to generate a dianion (Figure 2D). In both monoanionic and dianionic mechanisms, the 2′OH is first deprotonated (at pre-equilibrium) before the nucleophilic attack and the departure of the leaving group proceed.

The nucleobase catalysis in the 2′OH activation has been studied theoretically only in the context of the hairpin ribozyme where a guanine (G8 residue) has an active or passive role.[16,24] Nevertheless, the results can probably be extended to the hammerhead ribozyme[35] or the glmS ribozyme[36,37] in which a guanine (G12 and G33, respectively) may have exactly the same role. Up to now, only two models have been proposed: the first one where the nucleobase (in an anionic state) from residue G8 has an active role via a dianionic mechanism, the second one where the same nucleobase has only a passive role via a monoanionic mechanism. Here, the nucleobase contributes to the electrostatic reorganization of the active site without chemical participation in the proton transfer necessary for activation. So, the reaction basically follows the path corresponding to the uncatalyzed reaction with a coupling between the proton transfer and the in-line attack. On the other hand, the nucleobase charged in an anionic state has an active role and acts as a general base (Figure 2F).

When the nucleobase can act at the same time as a general base and as a proton donor (enol tautomer), the two chemical processes corresponding to the 2′OH activation and the nucleophilic attack may not be coupled in the monoanionic mechanism. Instead, the 2′OH activation can be coupled to another proton transfer from the enol group of the nucleobase to the close nonbridging oxygen (Nu-GB^{mono}). This is an alternative and new model proposed here (Figure 2E). Finally, the presence of a metal ion close to the 2′OH was shown to have an effect on the acidity of the alcoholic proton.[12] Thus, the presence of two catalysts, a metal ion in the outer-sphere coordination to facilitate the proton transfer and a nucleobase to take an active role in the activation, can have a synergic effect. A new activation model is proposed on the basis of this hypothesis (Figure 2G).

1. Metal-Dependent Activation. The full reaction paths are described as decomposed into three major steps: preactivation, activation, and postactivation (in-line attack and departure of the leaving group), in the monoanionic or dianionic mechanisms (Figures 3 and 4).

1.1. Preactivation or Metal-Dependent Conformational Changes. Reaction Paths. The preactivation involves some conformational changes that are driven by the conversion from an outer-sphere to an inner-sphere metal coordination to the 2′-oxygen through a pentacoordinated metal intermediate. The starting structure involves a hexacoordinated metal where the first coordination sphere (represented explicitly) is filled with five water ligands and only one RNA-like ligand: the nonbridging oxygen pro-R_P of the phosphate group. In the preactivated structure, one of the water ligands has been displaced by the 2′-oxygen that is inserted into the first coordination sphere that thus includes one water ligand less and one RNA-like ligand more. The rate-limiting step is the decrease in the metal coordination number n from $n = 6$ to $n = 5$. In the monoanionic mechanism, the preactivation is a stepwise process with the formation of a pentacoordinated metal including four

dx.doi.org/10.1021/jp200970d |J. Phys. Chem. B XXXX, XXX, 000–000

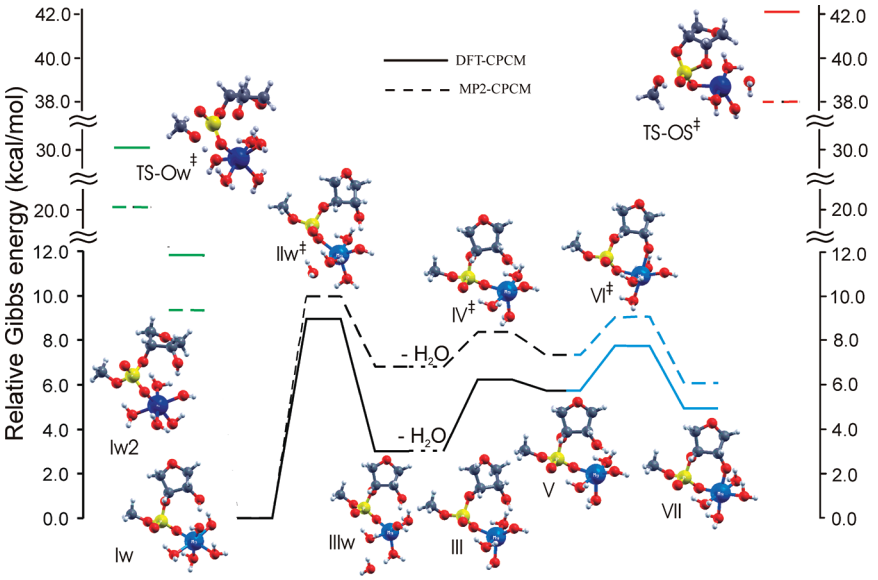

Figure 4. Gibbs free energy surface for the dianionic pathway (Me-GB^{di} activation modes). The black lines correspond to the preactivation step (structures from Iw to V). The blue line corresponds to the 2′OH activation, and the red line corresponds to the rate-determining transition state TS-OS‡ for the final cleavage reaction in the Me^{i}-GB^{di} pathway. The structures Iw2 and TS-Ow‡ (green line) correspond to the Me^{o}-GB^{di} mechanism of the cleavage reaction.[11] See the text for a more detailed description of the stationary points. Lines: full, DFT-CPCM pathway; dashedm MP2-CPCM pathway.

water ligands in the first shell and one excluded water ligand in the second shell (Figure 3, IwH to IIIwH). The second step restores a hexacoordinated metal through the inner-sphere coordination to the 2′-oxygen (IIIH to VH). In the dianionic mechanism (Figure 4), one of the water ligands is replaced by a hydroxide ion but the reaction path remains unchanged with respect to the monoanionic mechanism (Iw to IIIw and III to V); an additional step leads to the deprotonation of the 2′OH by the metal−hydroxide complex (V to VII). The structural and energetic changes involved in both the mono- and dianionic mechanisms are described in detail in the Supporting Information (sections S1 and S2, Tables S1 and S2).

Hydroxide Ion/Water Ligands: Dianionic/Monoanionic Pathways. The monoanion and dianion reactants IwH and Iw have a similar geometry but the repulsion between the water ligands is increased due to the presence of the negative charge from the hydroxide ion. The coordination distances are increased by 0.038 Å to a mean value of 2.162 Å in Iw compared to IwH (Tables S1 and S2, Supporting Information). It is in agreement with previous findings on the correlation between the coordination distances and the ligand charges.[38] Coordination bonds with water ligands involved in internal H-bonding are generally stronger and even more perceptive to the charge of the ligands (increase by 0.071 Å to a mean coordination distance of 2.156 Å, Table S2, Supporting Information).

In the gas-phase DFT calculations, the presence of a hydroxide ligand in the first coordination sphere ion displaces the equilibrium in favor of the pentacoordinated $[Mg(H_2O)_4\cdot(OH)]^+\cdots(H_2O)$ complex over the standard hexacoordinated $[Mg(H_2O)_5\cdot(OH)]^+$ complex. It is noteworthy that no minimum can be found for the hexacoordinated $[Mg(H_2O)_5(OH)]^+$ complex in the gas phase (B3LYP/aug-cc-pVTZ).[39] In fact, the pentacoordinated complex is formed by a spontaneous migration of one of the water ligands from the first to the second coordination shell.[39] The decrease in the coordination number is driven by the repulsion between the permanent and induced dipoles of the ligands and by Pauli repulsion,[40] but charge-transfer effects are not significant for the Mg^{2+} ion. A minor influence of charge-transfer effects for Mg^{2+} ion was also reported in the comparison of stabilities between octahedral and tetrahedral complexes of Mg^{2+} and Zn^{2+}.[41,42]

However, it is difficult to extend the observations on simple solvated Mg^{2+} ions to more complex systems. In the Iw structure two charged ligands are present: a hydroxide ion and a charged RNA-like ligand (Figure 4). The pentacoordinated dianionic intermediate (IIIw) is less stable than the hexacoordinated dianion (Iw) reactant ($\Delta G_{Iw\text{-}IIIw}$ = 3.0 kcal/mol, Table 3) whereas the monoanionic intermediate (IIIwH) is more stable than its corresponding hexacoordinated monoanion (IwH). The Gibbs free energy barrier associated with the formation of IIIw is 9.0 kcal/mol in DFT calculations (IIw) and even more pronounced in MP2 calculations (10.0 kcal/mol). By comparison, the Gibbs free energy barriers are at least 3 kcal/mol more favorable in the monoanionic mechanism (IwH to IIIwH, Table 2). Thus, the monoanionic preactivation is more favorable than the dianionic preactivation both from the kinetic and thermodynamic viewpoints (Tables 2 and 3).

In the monoanionic mechanism, a higher tendency to lower the coordination number of the Mg^{2+} ion can be explained in terms of reorganization energy (Figure S1, Supporting Information). The transition from a hexacoordinated to a pentacoordinated metal complex involves a rearrangement of four ligands from a square planar to a trigonal planar (three inner-sphere and one outer-sphere ligands) configuration, thus converting the octahedral into a trigonal bipyramidal geometry (Figure S1, Supporting Information). Both hexacoordinated metal complexes deviate from an ideal octahedral geometry: the distortion is located at the position of the hydroxide ligand and its neighbors for Iw and is more regularly distributed for IwH. One can expect that the reorganization energy is minimized when the coordination angles between the three ligands that are kept in the

dx.doi.org/10.1021/jp200970d |J. Phys. Chem. B XXXX, XXX, 000–000

Table 2. Relative Energies, Differences in Thermodynamic Corrections, and Relative Gibbs Free Energies (at 298 K) of the Stationary Points for the Monoanionic Activation Pathway and of Other Relevant Structures (Me-GB^{mono} Activation Modes)

structure[a]	ΔE (DFT)[b]	ΔE (MP2)[c]	ΔE_{ZPE}	ΔE_{TRV}	$-T\Delta S$	ΔE_{solv}-CPCM	ΔG_{tot}-DFT/CPCM[d]	ΔG_{tot}-MP2/CPCM[e]
IwH[f]	0.0	0.0	0.0	0.0	0.0	0.0	0.0	0.0
IIwH‡	7.1	8.6	−0.5	−0.3	0.1	−1.2	5.1	6.7
IIIwH	−0.1	3.6	0.1	−0.0	−0.7	−1.8	−2.5	1.1
IIIH[g,h]	0.0	0.0	0.0	0.0	0.0	0.0	0.0	0.0
IVH‡	4.2	2.3	0.2	−0.5	−1.7	1.7	7.2	5.3
VH	2.1	−1.8	0.4	−0.0	−1.0	1.5	4.9	1.0
VH-OR	14.1	12.7	−0.9	−0.4	−1.6	−7.2	7.1	5.6
VH-OS	4.3	−0.7	0.4	0.0	−1.1	2.3	8.1	3.1
VIH-OR‡	18.9	16.8	−2.7	−0.5	−1.5	−3.5	13.7	11.7
VIH-OS‡	13.2	7.6	−1.9	−0.3	−1,6	5.8	18.4	12.9
VIIH-OR	17.6	16.2	−0.1	−0.3	−1.1	−1.0	17.3	15.8
VIIH-OS	13.2	8.1	−0.6	0.2	−0.6	6.1	19.4	14.3
VIIH-O3	36.2	33.3	−1.1	0.6	1.7	6.9	41.0	38.1
TSH-O3‡	57.6	48.4	−2.5	−0.4	−1.7	3.0	59.5	50.3
TSH-OR‡	48.6	39.8	−2.6	−0.4	−1.6	1.5	48.7	39.9
TSH-OS‡	45.6	37.0	−2.4	−0.4	−1.8	2.8	47.3	38.8
INT	27.4	22.6	−0.5	0.5	−1.6	−0.3	25.6	20.7
TS-2‡	27.3	24.1	−1.0	0.2	1.1	−2.8	22.5	19.3
PROD	−2.6	−0.8	0.4	−0.0	1.2	2.7	−0.8	1.1

[a] Structures marked with a ‡ are transition states and the other states are minima on the potential energy surface. [b] B3LYP/6-311+G(2d,2p)//B3LYP/6-31+G* values in kcal/mol. [c] MP2(FC)/6-31+G**//B3LYP/6-31+G* values in kcal/mol. [d] B3LYP-CPCM/6-311+G(2d,2p)//B3LYP/6-31+G* values in kcal/mol. [e] B3LYP/6-31+G* ZPE, thermal, and Gibbs energy corrections and B3LYP-CPCM/6-311+G(2d,2p)//B3LYP/6-31+G* solvation corrections are considered. [f] The calculated values of energies for IwH are E(DFT) = −1572.029354 hartree, E(MP2) = −1567.786332 hartree, ZPE = 0.296896 hartree, E_{TRV} + Δ(pV) = 17.53 kcal/mol, S = 177.1 cal/(mol·K), E(DFT-CPCM) = −1572.108361. [g] Structure IIIwH is considered to be equivalent to structure IIIH. In structure IIIH a water molecule in the second coordination shell of Mg^{2+} is missing as compared to structure IIIwH. The relative energy for structure IIIH is zeroed here. The relative energies of structures IIIH, IVH, VH, VIH-OR, VIH-OS, VIIH-O3, VIIH-OR, VIIH-OS, TSH-O3, TSH-OR, TSH-OS, and PROD on Figure 3 are the sums of their relative energies with respect to the IIIwH structure and relative energy of the IIIH structure. [h] The calculated values of energies for IIIH are E(DFT) = −1495.542982 hartree, E(MP2) = −1491.704672 hartree, ZPE = 0.271123 hartree, E_{TRV} + Δ(pV) = 15.93 kcal/mol, S = 167.3 cal/(mol·K), E(DFT-CPCM) = −1495.630700.

inner-coordination sphere (ligands labeled 1, 2, and 3: Figure S1, Supporting Information1) in the trigonal plane are as close to 120° as possible. The mean angle change between these ligands when going from IwH to IIIwH and from Iw to IIIw is 22.6° and 36.8°, respectively. So, the difference in energy barrier between the monoanion and the dianion for the transition from a hexacoordinated to a pentacoordinated metal complex can be explained in terms of reorganization of the metal ligands. It will depend on how close they are from the trigonal bipyramid and how easy they can be rearranged. Previous studies on hydrated Mg^{2+} complexes suggest the results obtained here using an explicit representation of the first hydration shell of the metal and an implicit representation (continuum model) for the other hydration shells gives a good description of the geometries and energetics.[29,43−46]

1.2. Activation Paths: Disconnected or Coupled Proton Transfer with the In-Line Attack. Me-GB^{mono} Pathways with a Coupled Proton Transfer and Subsequent Reaction Steps. In the monoanionic mechanism, the proton transfer is intramolecular and the catalyst is an internal general base (Figure 1). Usually, it is one of the nonbridging oxygens (pro-R_P or pro-S_P) of the phosphate group as proposed in the uncatalyzed reaction[14] or in the catalyzed reaction of the hairpin ribozyme.[16] Alternatively, the 3′O bridging oxygen may be used as a general base as well but this reaction path was never described before (Figure 2B). The three Me-GB^{mono} pathways follow a preactivation as described above for the monoanionic mechanism (Figure 3). The proton is transferred to the 3′-oxygen or either of the two nonbridging oxygens and leads to the formation of monoanionic intermediates; the reaction may then go forward with the in-line attack of the activated nucleophile on the phosphorus atom. In the Me-GB^{mono} pathways, this is the rate-limiting step of the reaction dissociated from the final step that corresponds to the departure of the leaving group (Figure 3). The more favorable energy barriers involve one of the two nonbridging oxygens as a general base (structures TSH-OS and TSH-OR); the less favorable pathway corresponds to the bridging 3′-oxygen as a general base with an energy barrier increased by 10 kcal/mol in the rate-limiting step (TSH-O3, Table 3). A more detailed description of the energetic and structural changes along the Me-GB^{mono} pathways can be found in the Supporting Information (section S3).

Me-GB^{di} Pathways: Inner/Outer-Sphere Coordination Spheres. In the dianionic mechanism, the preactivation has a higher energy barrier, as described previously. The activation per se involves the metal−hydroxide complex as general base to activate the 2′OH nucleophile (Figure 4). This particular chemical step (V to VII) has a modest energy barrier; thus the activation is dominated by the energy cost of the preactivation (Table 3). A reaction pathway based on a Me-GB^{di} mode of activation has been proposed in a single-metal-ion model of catalysis for the hammerhead ribozyme.[11] In this model, the activation proceeds without preactivation because the 2′-oxygen remains in the outer-coordination sphere of the metal for the activation and the subsequent reaction

Table 3. Relative Energies, Differences in Thermodynamic Corrections, and Relative Gibbs Free Energies (at 298 K) of the Stationary Points for the Dianionic Activation Pathway and of Other Relevant Structures (Me-GB^{di} Activation Modes)

structure[a]	ΔE(DFT)[b]	ΔE(MP2)[c]	ΔE_{ZPE}	ΔE_{TRV}	$-T\Delta S$	ΔE_{solv}-CPCM	ΔG_{tot}-DFT/CPCM[d]	ΔG_{tot}-MP2/CPCM[e]
Iw[f]	0.0	0.0	0.0	0.0	0.0	0.0	0.0	0.0
IIw‡	5.3	6.3	−0.5	−0.0	−0.4	4.6	9.0	10.0
IIIw	−1.5	2.3	0.3	−0.1	−0.5	4.7	3.0	6.8
Vw	−1.7	−2.3	−0.9	−0.2	0.1	7.1	4.4	3.75
VHOH	−1.7	−2.3	−0.9	−0.2	0.1	7.1	4.4	3.75
VIw‡	−1.1	−2.6	−2.4	−0.5	1.1	7.3	4.35	2.9
VIIw	−2.9	−4.5	−0.2	0.1	0.0	6.4	3.4	1.8
Vw2‡	−0.9	−1.2	−2.6	−0.4	0.4	7.6	4.2	4.0
Vw3	−1.6	−1.8	−0.8	0.2	−0.6	7.15	4.2	4.1
Iw2[g]	10.0	7.5	0.1	0.3	−0.5	1.9	11.8	9.3
TS-Ow‡[h]	38.9	28.3	−2.5	−0.9	3.0	−7.7	30.9	20.3
III[i,j]	0.0	0.0	0.0	0.0	0.0	0.0	0.0	0.0
IV‡	0.8	−0.6	−0.6	−0.3	0.8	2.5	3.2	1.8
V	0.7	−1.2	−0.5	0.2	−0.5	2.8	2.7	0.8
VI‡	2.7	1.0	−2.35	−0.5	1.6	3.3	4.7	3.0
VII	−1.6	−4.6	−0.1	−0.1	0.8	3.0	1.9	−1.1
TS-OS‡	36.9	29.0	−2.6	−0.7	2.2	6.5	39.1	31.2
III-2	−0.5	−0.2	0.2	−0.2	0.5	−1.3	−1.4	−1.1
IV-2‡	1.6	1.9	−0.8	−0.4	1.2	1.3	2.8	3.1
V-2	0.25	−0.7	−0.4	−0.1	0.7	3.0	3.4	2.5
VI-2‡	3.6	2.3	−2.8	−0.4	1.6	2.3	4.2	2.9

[a] Structures marked with a ‡ are transition states and the other states are minima on the potential energy surface. [b] B3LYP/6-311+G(2d,2p)//B3LYP/6-31+G* values in kcal/mol. [c] MP2(FC)/6-31+G**//B3LYP/6-31+G* values in kcal/mol. [d] B3LYP-CPCM/6-311+G(2d,2p)//B3LYP/6-31+G* values in kcal/mol. [e] B3LYP/6-31+G* ZPE, thermal, and Gibbs energy corrections and B3LYP-CPCM/6-311+G(2d,2p)//B3LYP/6-31+G* solvation corrections are considered. [f] The calculated values of energies for Iw are E(DFT) = −1571.624349 hartree, E(MP2) = −1567.56780 hartree, ZPE = 0.286200 hartree, E_{TRV} + Δ(pV) = 16.32 kcal/mol, S = 166.7 cal/(mol·K), E(DFT-CPCM) = −1571.651043. [g] Iw2 structure corresponds to the reoptimized reactant I structure from ref 11. [h] TS-Ow‡ structure corresponds to the reoptimized TS2 structure from ref 11. [i] Structure IIIw is considered to be equivalent to structure III. In structure III a water molecule in the second coordination shell of Mg^{2+} is missing as compared to structure IIIw. The relative energy for structure III is zeroed here. The relative energies of structure III−VII and III-2, IV-2, V-2, and VI-2 in Figures 4 and S2 (Supporting Information) are the sums of the IIIw energy and the relative energy of the structure with respect to structure III. [j] The calculated values of energies for III are E(DFT) = −1495.141387 hartree, E(MP2) = −1491.304434 hartree, ZPE = 0.260647 hartree, E_{TRV} + Δ(pV) = 15.08 kcal/mol, S = 160.2 cal/(mol·K), E(DFT-CPCM) = −1495.162793.

steps. Although the reaction follows a dianionic mechanism, the proton transfer and the in-line attack are coupled as proposed and reminiscent of monoanionic mechanisms. On the other hand, the proton transfer is disconnected from the in-line attack in the model proposed here.

To analyze the influence of the inner or outer-coordination sphere on the activation modes Me^{i}-GB^{di} or Me^{o}-GB^{di}, the structure Iw was used as reference. A detailed comparison between Iw and the reactant Iw2 proposed in a previous study[11] is given in the Supporting Information (section S4, Table S3 and Figure 3S). Iw is more stable than Iw2 in the Me^{o}-GB^{di} pathway.[11] Hence, Iw2 is not a global minimum and appears to be already in some "pre-activated" state (Figure 4). The metal ion is more tightly bound to the RNA-like ligand in Iw and would require a reorganization of its hydrogen bond network to be converted into Iw2 with a Gibbs free energy penalty around 10 kcal/mol (Table 3).

In the Me-GB^{di} paths, the reaction requires at least two successive proton transfers: the first one for the 2′OH activation to proceed with the in-line attack, the second for the protonation on the 5′-oxygen to facilitate the departure of the leaving group. In the Me^{o}-GB^{di} mode, the hydroxide ion/metal complex activates the 2′OH before another proton from the hydrated metal is transferred to the 5′ leaving group. Although the first proton transfer has a high energy barrier (as shown previously[11]) because it is coupled with the in-line attack, the rate-limiting step remains associated with the second proton transfer. So, taking into account the preactivation to go from Iw (stable hexacoordinated reactant) to Iw2 (predisposed for activation and in-line attack), the overall energy barrier rises to 31 kcal/mol (TS-Ow, Table 3, Figure 4) corresponding to an increase of about 10 kcal/mol with respect to the single-metal-ion model of catalysis.[11] In the Me^{i}-GB^{di} mode, the preactivation and activation have low energy barriers (9−10 kcal/mol). However, the subsequent reaction steps require one additional proton transfer to complete the reaction. With two inner-sphere coordinations to the RNA-like ligand, the hydrated Mg^{2+} ion has no direct interaction with the leaving group. Thus, the protonation of the leaving group has to proceed in two steps: a proton is first transferred from a water ligand to one the nonbridging oxygens and then it is transferred to the 5′-oxygen. The latter proton transfer is still the rate-limiting step (TS-OS, Figure 4) but the energy barrier is further increased, resulting in an overall energy barrier of 39 kcal/mol (Table 3) equivalent to the typical barrier estimated for the uncatalyzed reaction.[47]

The catalytic power of the metal ion as the only catalyst in the reaction varies significantly depending on the coordinations with the RNA-like ligand (inner/outer-sphere coordinations) having

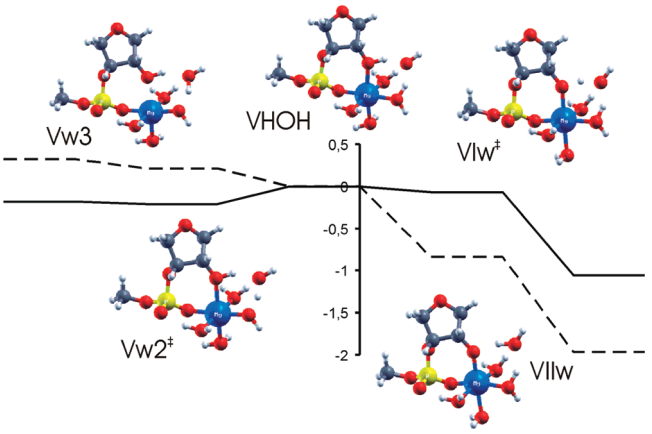

Figure 5. Gibbs free energy surface for the activation of the metal coordinated 2′OH group by a specific base (Me-SB activation mode). The competing deprotonation of a water ligand is shown for comparison (structures Vw2 and Vw3). Lines: full, DFT-PCM pathway; dashed, MP2-PCM pathway. Realtive Gibbs energy (vertical axis) is in kcal/mol.

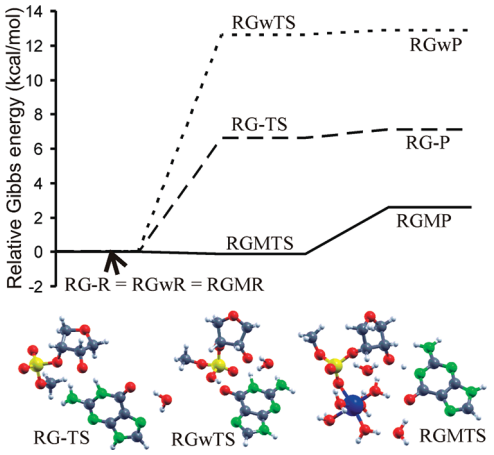

Figure 6. Gibbs free energy surfaces for activation of the 2′OH group by G_{DP} (dashed line), by G_{NE} (dotted line), and by G_{DP} (full line) in the presence of the hydrated Mg^{2+} ion (Nu-GB and Nu+Me-GB activation modes). Only structures of transition states are shown. Structures of reactants and products (Figure S4, Supporting Information) do not show significant changes of the positions of the atoms except for the transferred proton.

an impact on the stabilization of the negative charge on the nonbridging oxygens[24] and on the pK_a modulation of the coordinated proton donor. Although the monoanionic mechanisms exhibit a more favorable preactivation, the energy barrier of the cleavage reaction is significantly lower when a metal−hydroxide complex is involved, orienting the reaction toward dianionic mechanisms. The presence of a specific base (hydroxide OH^- anion) may decrease the barrier height of an equivalent cleavage pathway by about 4.5 kcal/mol (see relative energies of equivalent TSH-OS and TS-OS structures in Tables 2 and 3, respectively). In the dianionic mechanism, the existence of various concurrent paths may be detrimental to the catalytic efficiency of the metal ions as catalysts.

Me-SB Pathway: "Monoanionic" Preactivation and "Dianionic" Activation. The Me-SB path is a mix combining the more favorable paths from the monoanionic and dianionic mechanisms for the preactivation and the 2′OH activation, respectively. It follows the monoanionic preactivation (IwH to VH, Figure 3). Then, a hydroxide ion in the metal outer-sphere coordination (VHOH) acts as a specific base to activate the 2′OH nucleophile (Figure 5!). A hydroxide ion was added to the second metal coordination shell in VH to obtain the VHOH structure (see Table 3 and Figure 5). Two concurrent processes are then possible depending on the proton donor: the 2′OH or an equatorial water ligand (for a more detailed description, see section S6 in the Supporting Information). In the first case, the reaction proceeds with the 2′OH activation without any apparent barrier. In the second case, the reaction leads to some intermediate (Vw3, Figure 5) equivalent to the preactivated metal−hydroxide complex in the dianionic mechanism (V, Figure 3B). The reaction may further proceed as in the dianionic mechanism for the activation. In the Me-GB^{di} path, the proton transfer has a small activation barrier of 2 kcal/mol (V to VI, Table 3), which is eliminated in the Me-SB path.

2. Nucleobase-Dependent Activation. *2.1. Active Participation of Nucleobases as Catalysts: Monoanionic/Dianionic Mechanisms.* The participation of a nucleobase as a catalyst in the 2′OH activation has been addressed in the models of catalysis proposed for the hairpin ribozyme.[16,24] Both the monoanionic and dianionic mechanisms have been studied where the nucleobase has a passive or active chemical role in the proton transfer, respectively. For the sake of comparison with those data, the same dianionic mechanism has been examined. On the other hand, an alternative pathway of activation corresponding to the monoanionic mechanism is also examined but where the nucleobase plays an active chemical role in the proton transfer. Moreover, a possible cooperative model based on the active participation of a nucleobase and the passive participation of a metal is also studied.

The 2′OH activation occurs through the proton transfer either to the anionic N1-deprotonated guanine (G_{DP}) (Nu-GB^{di} pathway) or to the neutral enol-tautomer of guanine (G_{NE}) (Nu-GB^{mono} pathway).[48] Indirect experimental evidence suggests the existence of G_{DP} in the active site of the hammerhead ribozyme.[49] In the cooperative model with a nucleobase and a metal catalyst (Nu+Me-GB^{di} pathway), the G_{DP} species is also involved in the activation of the 2′OH, which is facilitated by the outer-sphere coordinated metal. The initial structure of the RNA moieties (including the nucleobase) were taken from the in-line conformation in the crystal structure of the full-length hammerhead ribozyme.[34] The in-line conformation was preserved in the activation pathways except for Nu-GB^{di} where the substrate moiety flipped back to a more usual RNA conformation (the geometries of the reactants and products are provided in Figure 4S, Supporting Information). In spite of this conformational difference for Nu-GB^{di}, the energy barriers between the three pathways can still be compared. In fact, recent evidence shows that the in-line conformation is not a decisive factor for the cleavage reaction[50] because it is responsible for a ∼12-fold increase of the cleavage rate. It corresponds to an activation barrier decrease of ∼1.5 kcal/mol, which is insignificant in comparison to the overall $\sim 10^{12}$ increase due to the enzyme environment[50] (i.e., activation barrier decreased by ∼16 kcal/mol). As shown in the three pathways (Figure 6), the proton transfer from the 2′OH group to the N1 imino nitrogen of guanine is always endergonic: the products are not stabilized with respect to the backward reaction when the thermochemical corrections are included (Table 4). Therefore, we will discuss only the

dx.doi.org/10.1021/jp200970d |J. Phys. Chem. B XXXX, XXX, 000–000

Table 4. Relative Energies and Gibbs Free Energies (at 298 K, in kcal/mol) of the Stationary Points for the Nucleobase-Dependent Activation Pathways[a] (Nu-GB and Nu+Me-GB Activation Modes)

structure	ΔE(DFT)	ΔE(MP2)	ΔE_{ZPE}	ΔE_{TRV}	$-T\Delta S$	ΔE_{solv}-CPCM	ΔG_{tot}-DFT/CPCM	ΔG_{tot}-MP2/CPCM
RG-R	0.0[b]	0.0[d]	0.0	0.0	0.0	0.0	0.0[f]	0.0[f]
RG-TS	10.1[b]	11.4[d]	−2.7	−0.5	−1.4	−1.6	6.6[f]	8.0[f]
RG-P	9.9[b]	13.5[d]	−1.1	−0.2	−0.1	−1.6	7.1[f]	10.6[f]
RGwR	0.0[b]	0.0[d]	0.0	0.0	0.0	0.0	0.0[f]	0.0[f]
RGwTS	11.7[b]	10.9[d]	−2.7	−0.6	−3.0	1.2	12.6[f]	11.8[f]
RGwP	12.0	11.7[d]	−1.7	−0.2	−1.6	1.1	12.9[f]	12.5[f]
RGMR	0.0[c]	0.0[e]	0.0	0.0	0.0	0.0	0.0[g]	0.0[g]
RGMTS	1.7[c]	1.4[e]	−2.5	−0.3	−0.6	0.4	−0.1[g]	−0.4[g]
RGMP	−0.9[c]	1.3[e]	3,0	−0.1	0.5	1.1	2.6[g]	4.8[g]

[a] See the text for the description. [b] Relative energies are based on B3LYP/6-311+G(2d,2p)//B3LYP/6-31+G*. [c] Relative energies are based on B3LYP/6-311+G(2d,2p)//HF/3-21+G*. [d] Relative energies are based on MP2(FC)/6-31+G**//B3LYP/6-31+G*. [e] Relative energies are based on MP2(FC)/6-31+G**//HF/3-21+G* values. [f] B3LYP-CPCM/6-311+G(2d,2p)//B3LYP/6-31+G* relative solvation energies with B3LYP/6-31+G* ZPE, thermal, and Gibbs energy corrections are considered. [g] B3LYP-CPCM/6-311+G(2d,2p)//HF/3-21+G* relative solvation energies with HF/3-21+G* ZPE, thermal, and Gibbs energy corrections are considered.

changes in reaction Gibbs energy (endergonicity) rather than Gibbs energy barriers.

The Nu-GB^{mono} reaction pathway is more endergonic than the two other reaction pathways: Nu-GB^{di} and Nu+Me-GB^{di}, which involve a single proton-transfer event. On the other hand, the Nu-GB^{mono} activation mode requires two concerted proton transfers for the 2′OH activation and the conversion of the enol to keto tautomer. In this second event, the proton donor is the O6-enol group and the proton acceptor the pro-S_p nonbridging oxygen. As a result, G_{NE} is converted into its standard tautomeric form and the overall change on the RNA-like substrate is equivalent to a GB^{mono} activation mode in the uncatalyzed reaction. The reaction path is similar when the stationary points are optimized using an implicit solvent model (CPCM/B3LYP/6-31+G* level), suggesting that the two concerted proton transfers can take place in solution as described in the activation model. The reaction is strongly endothermic: ΔG_r^0 = 12.9 kcal/mol (Figure 6) but the energy barrier can be considered slightly underestimated because the reactant is taken in a minor tautomeric form. An energy correction of 1.1 kcal/mol may be applied to account for the energy barrier to displace the guanine into its enol tautomeric form,[16] raising the overall Gibbs energy difference to $\Delta G_r^0 \approx$ 14 kcal/mol. The reaction path is somehow similar to the Nu-GB^{mono} activation mode described for the hairpin ribozyme[16,24] where the proton is transferred to one of the two nonbridging oxygens (Nu-GB^{mono}-OR or Nu-GB^{mono}-OS). Here, the proton is transferred specifically to the pro-S_p oxygen but no significant difference is expected for the transfer to the pro-R_p oxygen. Although the nucleobase does play an active chemical role in this case, the Gibbs energy difference associated with the formation of the activated intermediate (RGwP, Figure 6) is equivalent to that calculated for an endothermic reaction following the Nu-GB^{mono}-OR or Nu-GB^{mono}-OS mode of activation: 14 and 11 kcal/mol, respectively.[16,24]

The activation Gibbs energy and the endergonicity of the reaction are strongly lowered when the catalyst is an anionic guanine (G_{DP}) and further if a metal catalyst is also present. The endergonicity is reduced by about half with a Gibbs energy difference of 7.1 kcal/mol in the presence of an anionic nucleobase (Nu-GB^{di}) and yet lowered to 2.6 kcal/mol in the presence of a metal (Nu+Me-GB^{di}). In the Nu+Me-GB^{di} pathway, the metal is directly coordinated to pro-R_P oxygen in the reactant (RGMR, Figure S4, Supporting Information). The 2′OH group lies in the second coordination sphere of the metal, which is hexacoordinated and includes two additional water molecules in the second hydration shell. One of the water molecules solvates the 2′OH group, the other one the O6-keto group from G_{DP}. The explicit solvation of the 2′OH group is ensured by two water molecules from the first and second hydration shells of the metal. In this model, the reaction has a well-balanced transition state where the proton is halfway from the proton donor and acceptor (Table 4).

2.2. Metal Ion as a Cocatalyst: pK_a Shift of the 2′OH Group. The comparison of the Nu+Me-GB^{di} and Nu-GB^{di} pathways suggests that the metal ion plays a major role in the decrease of the activation energy and endergonicity of the 2′OH activation by the nucleobase. The endergonicity of the process is lowered by 4.5 kcal/mol, which corresponds to a decrease in pK_a by 3.3 log units. The presence of several water molecules in the first or second coordination spheres of the metal makes the 2′OH group more explicitly solvated in Nu+Me-GB^{di} compared to Nu-GB^{di}.

To determine more precisely the role of the metal and the solvation of the 2′OH on the activation, complementary calculations were performed on the reactant and products (RGM-R and RGM-P, Figure 4S, Supporting Information). In the first series of calculations, the Mg^{2+} ion was replaced by point charges on a scale between 0.0e and +3.0e; the difference in electronic energy between the two structures was calculated by single point energy calculations without optimization. In the second series of calculations, the Mg^{2+} ion was first replaced by a monovalent Li^+ ion (metal charge reduction) and then removed (metal charge cancellation). The resulting structures were fully optimized but preserved the interactions between the water molecules in the initial structures in the presence of a divalent ion.

Either way, the endergonicity of the proton transfer is linearly dependent on the charge obeying Coulomb's law (Figure 7). The slope of the energy/charge variation is much higher for the point charges because here a reorganization of the solvent molecules and charge-transfer effects are not allowed. The increasing charge on the 2′O atom polarizes the first coordination shell of the metal. However, no change in charge transfer between the solvated metal and the 2′-oxygen was observed. Thus, the activated $2'O^{(-)}$ group is stabilized purely by electrostatic forces. The results are consistent for both ways to vary the metal charge: whether the

dx.doi.org/10.1021/jp200970d |J. Phys. Chem. B XXXX, XXX, 000–000

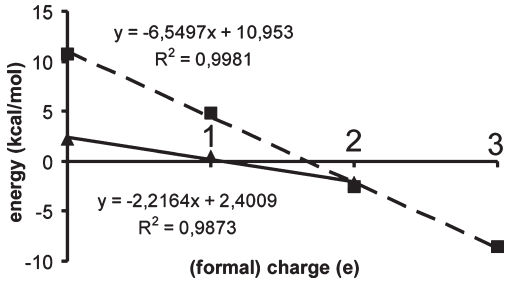

Figure 7. Endergonicity versus charge in the Nu+Me-GB activation mode. Gibbs free energies are calculated on the B3LYP-CPCM/6-311+G(2d,2p)//B3LYP/6-31+G* level. Dashed line: the point charges are placed on the Mg^{2+} positions in the RGMR and RGMP structures, no optimizations were performed, and only the change in electronic energy between the reactant and product structures is considered. Full line: formal charges +2 and +1 are represented by the optimized structures with Mg^{2+} and Li^{+} ions. The metal ion was taken out to represent +0 formal charge. The structures were fully optimized and thermal corrections to energy were considered.

Gibbs energy is calculated for a divalent ion or extrapolated from the calculations on the monovalent ion. The Li^{+} and Mg^{2+} ions lower the endergonicity of the proton transfer by 1.78 and 4.43 kcal/mol, respectively. The pK_a value is decreased accordingly by 1.31 and 3.25 log units. The endergonicities of the 2′OH activation, as calculated above for the end points of the charge scale (corresponding to the absence or presence of a divalent ion: 0.0 and +2.0e), correlate very well with the reaction free energies in the Nu+Me-GB^{di} or Nu-GB^{di} pathways. It suggests that the metal acts via nonspecific electrostatic interactions[51] as a cocatalyst to increase the acidity of the proton and facilitate the 2′OH activation by a nucleobase.

DISCUSSION

The roles of the metal and nucleobase catalysts can be inferred from the comparison between the catalyzed and uncatalyzed reactions. For each reaction mechanism, the catalysts can also be evaluated with respect to the activation step for their catalytic efficiency and for their influence on the reaction pathway. Finally, some insights may be gathered on the influence of the active site environment by the comparison between QM and QM/MM models, whether the active site is represented only by the catalyst(s) or by the catalysts included in the full ribozyme, respectively. However, the comparison between different studies on a given activation mode can be tricky because the 2′OH activation may be concerted or not with the in-line attack (monoanionic mechanism). Thus, the Gibbs energy differences to compare are those of the in-line attack, which include the 2′OH activation. On the other hand, the preactivation is not included in the previous studies, as described above. So, energy corrections are applied when necessary for a fair comparison.

In the monoanionic mechanism, both the metal and the nucleobase catalysts facilitate the 2′OH activation with respect to the uncatalyzed reaction. The nucleobase catalyst can lower the energy barrier by 7 kcal/mol for two variants of the Nu-GB^{mono} activation mode: Nu-GB^{mono}-OR/GB^{mono}-OR or Nu-GB^{mono}-OS/GB^{mono}-OS (Table 5). In the current study, only the Nu-GB^{mono}-OS mode has been evaluated; the catalytic efficiency is slightly weaker: 5 kcal/mol (Nu-GB^{mono}-OS/GB^{mono}-OS). As for the metal catalysts, the different Me-GB^{mono} modes (-O3, -OR, -OS) require some rearrangements for the proton to be transferred on any of the three proton acceptors: the 3′O bridging or pro-R_p or pro-S_p nonbridging oxygens (Figure 3). These rearrangements may include coordination changes such as the loss of the inner-sphere coordination with the nonbridging oxygen and the formation of a pentacoordinated metal (VIIH-OR). The metal catalysts lower the energy barrier but by 5 kcal/mol in the most favorable case (Me-GB^{mono}-OR/GB^{mono}-OR, Table 5). Taken together, the data suggest a nucleobase is slightly more efficient for the 2′OH activation.

The Nu-GB^{mono}-OS examined here does involve an active chemical role of the nucleobase, but the corresponding energy barrier is a bit higher (2 kcal/mol) than what has been reported previously in a QM/MM model.[16] Half of the energy difference between the two models is due to the energy cost for converting the guanine to its active tautomeric form (1.1 kcal/mol). The other half is probably due to the difference in the reaction path. A single internal proton transfer is involved from the 2′OH to one of the two nonbridging oxygens (with no chemical role of the nucleobase) in Nu-GB^{mono}-OS. Two concerted proton transfers are involved from the 2′OH to the N1-imino of guanine and from the O6-enol group and to the nonbridging oxygen in Nu-GB^{mono}. In this latter case, the nucleobase has an active chemical role as a general acid/base (Figures 6 and 4S, Supporting Information). The similar energy barrier between the two models (Nu-GB^{mono}/ Nu-GB^{mono}-OS: 14 kcal/mol vs 12 kcal/mol) suggests that the nucleobase can still have a chemical role in the proton transfer in the monoanionic mechanism. The presence of the nucleobase alone, whether it has a chemical role or not (QM model vs QM/MM model, Table 5), is sufficient to lower significantly the energy barrier of the uncatalyzed reaction. Thus, the nucleobase environment should provide a proper arrangement of the catalyst in the active site for the 2′OH activation and the following chemical steps, but it may not have any additional positive contribution, at least in the case of the hairpin ribozyme. We may expect a different trend in the case of metal catalysts, which are very dependent on the environment for binding.

Putting in perspective the 2′OH activation with the RNA catalysis, one may compare the energy barriers for the rate-limiting step depending on the catalytic strategy. The 2′OH activation represents an energy cost important with respect to the energy barrier of the rate-limiting step in the nucleobase catalysis (Nu-GB^{mono}), as shown in previous studies (Table 5). The nucleobase catalysis (Nu-GB^{mono}: -OR, -OS) appears to be generally more efficient than the metal ion catalysis, which cannot match the same efficiency (Me-GB^{mono}: -OR, -OS, -O3). However, such comparison is partly biased by the fact that what is attributed to the nucleobase catalysis includes the whole contribution from the active site, which may or may not be significant to facilitate the catalysis depending on the reaction step (see discussion above on 2′OH activation in the hairpin ribozyme). Besides, the presence of two metal catalysts appears to facilitate even more the 2′OH activation in a cooperative way (Me_2-GB^{mono}: 6.9 kcal/mol) but the energy barrier of the rate-limiting step in this reaction pathway is much larger (Table 5). The absence of the active site environment in this two-metal-ion model probably leads to an overestimation of the energy barrier. Although the nucleobase is more efficient as a single catalyst, the active site of self-cleaving ribozymes is likely evolutionary optimized to accommodate a specific catalyst.

In the dianionic mechanism, the 2′OH activation is generally omitted because it is not rate-controlling. The energy barrier was

dx.doi.org/10.1021/jp200970d |J. Phys. Chem. B XXXX, XXX, 000–000

Table 5. Comparison of the Relative Gibbs Free Energies for the Nucleophile Activation from Previous and Current Studies[a]

activation mode	ΔG_{aq} (B3LYP)	ΔG_{aq} (CP)	stationary points in proton transfer	ΔG_{aq} rate-limiting step
		Data on Uncatalyzed Reaction in Solution		
GB^{mono}-TS-OR¶	21−22[b]		PROD to TS2[exo/endo b]	44[b]
	(25−26)*		(a) to (b) (Figure 7)[c]	
		17[c]		58[c]
GB^{mono}-TS-OS¶	19[d]	NA	R to TS_{PT1}	38[d]
		Published Data on Different Mechanisms and Activation Modes		
Me-GB^{mono}	NA	NS	NA	56[e]
Me^{o}-GB^{di}	19*[f]		reactant to TS1	21
	(≥28)§,†			(31)[g]
		13[c]	(a) to (b) (Figure 9)	49[e]
Me_2-GB^{mono}	NA	6.9[e]	(a) to (b) (Figure 3)	45[e]
Me_2-GB^{di}	2.6[h]		I to II† [h]	11
	(≥13)†			(≥20)[g]
		5.4[e]	(a) to (b) (Figure 7)[e]	42
Nu-GB^{mono}-TS-OR¶	15[i]	NA	R to TS_{PT1} (O1P path)	25
	(15)*			
Nu-GB^{mono}-TS-OS¶	12[i]	NA	R to TS_{PT1} (O2P path)	21
	(14)*			
Nu-GB^{di} *	15*,[i]	NA	R to TS_{PT1} (N1 path)	27
		Data from the Current Study		
Me-GB^{mono}-TSH-OR	17	NA	VIIH-OR	49
Me-GB^{mono}-TSH-OS	19	NA	VIIH-OS	47
Me-GB^{mono}-TSH-O3	41	NA	VIIH-O3	60
Me^{i}-GB^{di}	9.0	NA	Iw to IIw	39
	(39)§,†			
Me^{i}-SB	5.1	NA	IwH to IIwH	39
	(39)§,†			
Nu-GB^{mono}	14[j]	NA	RGwR to RGw-TS	NA
Nu-GB^{di}	7.1[k]	NA	RG to RG-TS to RG-P	NA
	(11)◇			
Nu+Me-GB^{di}	2.6	NA	RGMR to RGMTS	NA

[a] The values in parentheses indicate a correction of the energy barrier: (*) energy barrier including the 2′OH activation and the in-line attack; (†) energy barrier including the 2′OH activation and the preactivation steps; (§) energy barrier including the 2′OH activation and the in-line attack and the departure of the leaving group; (¶) QM/MM calculations including the full ribozyme structure; (◇) energy barrier including the conformational rearrengement for the in-line attack. NA: not available. NS: not specified. All energies are in kcal/mol. [b] B3LYP/6-311++G(3df,2p)//B3LYP/6-31++G(d,p).[14] [c] CP (HCTH);[12] [d] B3LYP/6-31++G(d,p)//B3LYP/6-31+G(d).[24] [e] CP (HCTH).[13] [f] B3LYP/6-311+G(2d,2p)//B3LYP/6-31G(d,p).[11] [g] The Gibbs energy barrier for the nucleophile activation[11] can be corrected by including the contributions from the metal binding and conformational rearrangements (Table 3: 11.8 kcal/mol for Iw-2). [h] B3LYP/6-31+G**//HF/3-21+G*.[15] [i] B3LYP/6-311++G(3df,2p)//B3LYP/6-31++G(d,p).[16] [j] B3LYP/6-311+G(2d,2p)//B3LYP/6-31+G*: the Gibbs energy barrier corresponds to the 2′OH activation by a nucleobase as catalyst (RGwR to RGwP via RGwTS: Table 4) including an energy correction for converting the standard guanine tautomer into its enol tautomer (1.1 kcal/mol[16]). [k] B3LYP/6-311+G(2d,2p)//B3LYP/6-31+G*: the Gibbs energy barrier corresponds to the 2′OH activation by a nucleobase as catalyst (RG-R to RG-P via RG-TS: Table 4). Calculated energy correction for the conversion of phospho-ribose units in RG-R and RG-P into an in-line conformation is 4.2 kcal/mol. The geometry of the phospho-ribose moiety of the residue C17 as found in the crystal structure (PDB ID: 2GOZ)[34] were taken as a reference in-line conformation.

estimated computationally to be around 21 kcal/mol for the reaction in solution.[52] Only the more recent studies, involving a nucleobase catalyst, treat explicitly this reaction step in a QM/MM model of the hairpin ribozyme.[16] On the basis of the estimation given above and the available data, the nucleobase catalyst would lower the energy barrier for the 2′OH activation by 7 kcal/mol (Nu-GB^{di}, Table 5). In the single-metal-ion models, the 2′OH activation may be coupled to the in-line attack when the 2′-oxygen is in the outer-sphere coordination of the metal (Me^{o}-GB^{di}, Table 5). Moreover, the classical DFT methods used for Me^{o}-GB^{di} did not take into account the preactivation steps. Thus, the activation barrier for Me^{o}-GB^{di} (B3LYP) is largely underestimated, as described above. On the other hand, the 2′OH activation is independent from the in-line attack in Car−Parrinello studies (CP: 13 kcal/mol, Table 5): the metal catalyst would then lower the activation barrier by 8 kcal/mol. The presence of the 2′-oxygen in the inner-sphere coordination (Me^{i}-GB^{di}) would make the 2′OH activation even more favorable with an energy barrier lowered by 12 kcal/mol. When the general base is replaced by a specific base, the energy barrier can still be reduced with respect to the uncatalyzed reaction by almost 16 kcal/mol (Me^{i}-SB, Table 5). In the two-metal-ion

dx.doi.org/10.1021/jp200970d |J. Phys. Chem. B XXXX, XXX, 000–000

models, the energy barrier for the 2′OH activation (including the preactivation steps for the DFT study) is between 5 and 13 kcal/mol, which is not very different from that calculated for the single-metal-ion model corresponding to Me^{i}-GB^{di} (9 kcal/mol) despite subtle differences in conformations and metal coordinations between the models (Table 5). Nevertheless, a single metal catalyst involved in the first steps of the reaction (2′OH activation and in-line attack) cannot play any significant role in the rate-limiting step of the reaction: the departure of the leaving group. The energy barrier for the subsequent rate-limiting step with a single metal catalyst are thus significantly larger than those calculated in the presence of two catalysts a fortiori when the models also include the active site environment (Nu-GB modes for the hairpin ribozyme).

In the presence of two distinct catalysts, the metal catalysts are expected to be more efficient than the nucleobase catalysts in the dianionic mechanism by facilitating the 2′OH activation and the in-line attack. Alternatively, both metals and nucleobases may act in concert in the 2′OH activation as shown in the Nu+Me-GB^{di} mode (Figure 6) where the energy barrier is even more favorable and 18 kcal/mol lower than that of the uncatalyzed reaction. In the hammerhead ribozyme, the current models largely support a catalytic strategy based on nucleobases as the main and essential catalysts for both the 2′OH activation/in-line attack and the departure of the leaving group. However, both computational and experimental studies suggested recently an active participation of metal catalysts either in the departure of the leaving group[23] or in the 2′OH activation/in-line attack,[53] respectively. A Nu+Me-GB mode may be involved where the nucleobase is a general base and the metal a Lewis acid and/or where the metal is a cocatalyst activating the nucleobase.[5] Other recent experimental data on the HDV ribozyme strongly support a role as a Lewis acid for the metal catalyst and a hydroxide ion as a specific base (Me-SB mode) for the 2′OH activation.[54] A nucleobase (G25) is also involved in this model as a cofactor for binding the metal catalyst on its hoogsteen face. In the hairpin ribozyme, two nucleobases act as catalysts, but it is not clear yet whether they have an active chemical role in the 2′-hydroxyl deprotonation or the 5′-oxygen protonation. This study does not provide any further argument because the Nu-GB^{mono} modes are equivalent whether the nucleobase has a chemical role as an enol tautomer or just facilitates the 2′OH activation through solvation and specific hydrogen-bonding interactions.[16]

CONCLUSIONS

The nucleophile activation is the first chemical step of the transphosphorylation. Although it is not the rate-determining step in the overall reaction in any of these ribozymes, it represents a significant energy cost with respect to the overall energy barrier, especially in the monoanionic mechanism. In the dianionic mechanism, the nucleophile activation is generally examined starting from a preactivated conformational or chemical state for the catalysts. So, the metal and nucleobase catalysts are available as general bases (metal−hydroxide complex or anionic guanine). Thus, the energy barrier of activation has generally been underestimated by not taking into account some nonchemical steps involved in the prior activation of the catalyst responsible for the 2′OH activation.

The 2′OH activation can involve different catalysts and follow different pathways, which can be combined into different modes of activation (Figure 1 and Table 1). A representative number of them has been explored in this study on the basis of the different models proposed for the catalytic strategies of self-cleaving ribozymes. Although most of the metal activation modes presented here have been previously evaluated using different methods (DFT or CP), the energy barriers calculated for the preactivation steps put in perspective the corresponding models of catalysis. The results on the activation by a metal catalyst suggest that a single catalyst is not efficient enough to lower the overall activation barrier as expected from the experimental data, even if the barriers are likely overestimated (due to the absence of the active site environment that may contribute to lower the energy barrier). The Me-SB activation mode appears to be the more favorable way to activate the 2′OH nucleophile and is probably effective in the HDV ribozyme.

The nucleobase catalysts are generally more efficient than the metal catalysts in the monoanionic mechanism, but their exact role in the catalysis is still unclear. The activation modes, evaluated in a previous study on the hairpin ribozyme, suggested the nucleobase may contribute to lower the energy barrier just by providing a favorable charge environment in the active site. In this study, an additional activation mode involving an enol tautomer of guanine with an active chemical role in the catalysis has been identified. However, the energy barrier for this activation mode is equivalent to that of the other three activation modes already proposed. Finally, the endergonic activation modes also suggest a single nucleobase catalyst is not efficient enough for the reaction to proceed, unless it is pushed due to the participation of another catalyst and/or the active site environment in the following exergonic reaction steps (online attack and departure of the leaving group).

The 2′OH activation can be potentiated using both kinds of catalysts: metals and nucleobases. The specific case presented here involves a nucleobase as a general base and a metal that promotes the activation through nonspecific long-range electrostatic forces.[51] Thus, the metal may be distant from the 2′OH group but effective on the 2′OH activation and may also act as a Lewis acid in the departure of the leaving group. Some recent data suggest this activation mode may be effective in the hammerhead ribozyme. Beyond the static picture given by this model, the metal may also contribute to rearrange the active site to orient and/or activate the nucleobase to act as a general base. Vice versa, the nucleobase may contribute to create a favorable binding site where the metal can act as a Lewis acid.

ASSOCIATED CONTENT

Supporting Information. Details on (1) the geometries of the stationary points (Tables S1, S2 and Figures S1, S2, S4), structures, and potential energie surfaces, especially on the structures Iw and Iw2 and of those related to the Me^{i}-GB^{di} and Me^{o}-GB^{di} mechanisms (section S4, Figure S3, Table S3); (2) the energy decomposition analysis (sections S1−S7 and Table S4), a detailed description of the monoanionic (section S1), dianionic (section S2), Me-GB^{mono} (section S3), Me-SB (section S6), and Nu-SB and Nu-GB (section S7) pathways. This material is available free of charge via Internet at http://pubs.acs.org

AUTHOR INFORMATION

Corresponding Author

*E-mail: Z.C., chval@jcu.cz; F.L., fabrice.leclerc@maem.uhp-nancy.fr.

■ ACKNOWLEDGMENT

This project was supported by grants from the Czech Science Foundation (204/09/J010) and from the Ministry of Education, Youth and Sports of the Czech Republic (grants ME09062 and CZ.1.07/2.3.00/09.0076: to Z.C. and D.C., respectively) and also by CNRS funding for young investigators (ATIP, France) (to Z.C. and F.L.). The calculations were performed mostly at the Metacentrum (Czech Republic, project MSM6383917201), partly at the "Centre Informatique National de l'Enseignement Supérieur" (CINES, France) and the "Institut du Développement et des Ressources en Informatique Scientifique" (IDRIS, France: Project IDRIS 061413). Access to these supercomputing centers is highly acknowledged.

■ REFERENCES

(1) Gordon, P. M.; Fong, R.; Piccirilli, J. A. *Chem. Biol.* **2007**, *14*, 607–612.
(2) Fedor, M. J.; Williamson, J. R. *Nat. Rev. Mol. Cell Biol.* **2005**, *6*, 399–412.
(3) Bevilacqua, P. C.; Yajima, R. *Curr. Opin. Chem. Biol.* **2006**, *10*, 455–464.
(4) Stahley, M. R.; Strobel, S. A. *Science* **2005**, *309*, 1587–1590.
(5) Leclerc, F. *Molecules* **2010**, *15*, 5389–5407.
(6) Fedor, M. J. *Annu. Rev. Biophys.* **2009**, *38*, 271–299.
(7) Cochrane, J. C.; Strobel, S. A. *Acc. Chem. Res.* **2008**, *41*, 1027–1035.
(8) Murray, J. B.; Dunham, C. M.; Scott, W. G. *J. Mol. Biol.* **2002**, *315*, 121–130.
(9) Hampel, K. J.; Burke, J. M. *Biochemistry* **2003**, *42*, 4421–4429.
(10) Martick, M.; Lee, T. S.; York, D. M.; Scott, W. G. *Chem. Biol.* **2008**, *15*, 332–342.
(11) Torres, R. A.; Himo, F.; Bruice, T. C.; Noodleman, L.; Lovell, T. *J. Am. Chem. Soc.* **2003**, *125*, 9861–9867.
(12) Boero, M.; Terakura, K.; Tateno, M. *J. Am. Chem. Soc.* **2002**, *124*, 8949–8957.
(13) Boero, M.; Tateno, M.; Terakura, K.; Oshiyama, A. *J. Chem. Theory Comput.* **2005**, *1*, 925–934.
(14) Lopez, X.; Dejaegere, A.; Leclerc, F.; York, D. M.; Karplus, M. *J. Phys. Chem. B* **2006**, *110*, 11525–11539.
(15) Leclerc, F.; Karplus, M. *J. Phys. Chem. B* **2006**, *110*, 3395–3409.
(16) Nam, K.; Gao, J.; York, D. M. *J. Am. Chem. Soc.* **2008**, *130*, 4680–4691.
(17) Mlýnský, V.; Banáš, P.; Hollas, D.; Réblová, K.; Walter, N. G.; Šponer, J.; Otyepka, M. *J. Phys. Chem. B* **2010**, *114*, 6642–6652.
(18) Lee, T. S.; Lopez, C. S.; Giambasu, G. M.; Martick, M.; Scott, W. G.; York, D. M. *J. Am. Chem. Soc.* **2008**, *130*, 3053–3064.
(19) Lee, T. S.; York, D. M. *J. Am. Chem. Soc.* **2008**, *130*, 7168–7169.
(20) Lee, T. S.; Giambasu, G. M.; Sosa, C. P.; Martick, M.; Scott, W. G.; York, D. M. *J. Mol. Biol.* **2009**, *388*, 195–206.
(21) Wei, K.; Liu, L.; Cheng, Y. H.; Fu, Y.; Guo, Q. X. *J. Phys. Chem. B* **2007**, *111*, 1514–1516.
(22) Banáš, P.; Rulíšek, L.; Hánošová, V.; Svozil, D.; Walter, N.; Šponer, J.; Otyepka, M. *J. Phys. Chem. B* **2008**, *112*, 11177–11187.
(23) Wong, K. Y.; Lee, T. S.; York, D. M. *J. Chem. Theory Comput.* **2011**, *7*, 1–3.
(24) Nam, K.; Gao, J.; York, D. M. *RNA* **2008**, *14*, 1501–1507.
(25) Frisch, M. J.; Trucks, G. W.; Schlegel, H. B.; Scuseria, G. E.; Robb, M. A.; Cheeseman, J. R.; Montgomery, J. A., Jr.; Vreven, T.; Kudin, K. N.; Burant, J. C. et al. *Gaussian 03*, Revision E.01; Gaussian, Inc.: Pittsburgh, PA, 2003.
(26) Schaftenaar, G.; Noordik, J. H. *J. Comput.-Aided Mol. Des.* **2000**, *14*, 123–134.
(27) Kokalj, A. *Comput. Mater. Sci.* **2003**, *28*, 155–168.
(28) Caminiti, R.; Licheri, G.; Piccaluga, G.; Pinna, G. *Chem. Phys. Lett.* **1979**, *61*, 45–49.
(29) Markham, G. D.; Glusker, J. P.; Bock, C. W. *J. Phys. Chem. B* **2002**, *106*, 5118–5134.
(30) Velde, G. T.; Bickelhaupt, F. M.; Baerends, E. J.; Guerra, C. F.; Van Ginsbergen, S. J. A.; Snijders, J. G.; Ziegler, T. *J. Comput. Chem.* **2001**, *22*, 931–967.
(31) Ziegler, T.; Rauk, A. *Theor. Chim. Acta* **1977**, *46*, 1–10.
(32) Schneider, B.; Kabeláč, M.; Hobza, P. *J. Am. Chem. Soc.* **1996**, *118*, 12207–12217.
(33) Schneider, B.; Kabeláč, M. *J. Am. Chem. Soc.* **1998**, *120*, 161–165.
(34) Martick, M.; Scott, W. G. *Cell* **2006**, *126*, 309–320.
(35) Lee, T. S.; York, D. M. *J. Am. Chem. Soc.* **2010**, *132*, 13505–13518.
(36) Klein, D. J.; Been, M. D.; Ferre-D'Amare, A. R. *J. Am. Chem. Soc.* **2007**, *129*, 14858–14859.
(37) Klein, D. J.; Ferre-D'Amare, A. R. *Science* **2006**, *313*, 1752–1756.
(38) Mayaan, E.; Range, K.; York, D. M. *J. Biol. Inorg. Chem.* **2004**, *9*, 807–817.
(39) Kluge, S.; Weston, J. *Biochemistry* **2005**, *44*, 4877–4885.
(40) Katz, A. K.; Glusker, J. P.; Beebe, S. A.; Bock, C. W. *J. Am. Chem. Soc.* **1996**, *118*, 5752–5763.
(41) Dudev, T.; Lim, C. *J. Am. Chem. Soc.* **2000**, *122*, 11146–11153.
(42) Dudev, T.; Lim, C. *Chem. Rev.* **2003**, *103*, 773–788.
(43) Pavlov, M.; Siegbahn, P. E. M.; Sandstrom, M. *J. Phys. Chem. A* **1998**, *102*, 219–228.
(44) Pye, C. C.; Rudolph, W. W. *J. Phys. Chem. A* **1998**, *102*, 9933–9943.
(45) Šponer, J. E.; Sychrovský, V.; Hobza, P.; Šponer, J. *Phys. Chem. Chem. Phys.* **2004**, *6*, 2772–2780.
(46) Šponer, J.; Burda, J. V.; Leszczynski, J.; Hobza, P. *J. Biomol. Struct. Dynam.* **1999**, *17*, 61–77.
(47) Nam, K.; Cui, Q.; Gao, J. L.; York, D. M. *J. Chem. Theory Comput.* **2007**, *3*, 486–504.
(48) Lippert, B. *Chem. Biodiversity* **2008**, *5*, 1455–1474.
(49) Thomas, J. M.; Perrin, D. M. *J. Am. Chem. Soc.* **2008**, *130*, 15467–15475.
(50) Min, D. H.; Xue, S.; Li, H.; Yang, W. *Nucleic Acids Res.* **2007**, *35*, 4001–4006.
(51) Sigel, R. K. O.; Pyle, A. M. *Chem. Rev.* **2007**, *107*, 97–113.
(52) Glennon, T. M.; Warshel, A. *J. Am. Chem. Soc.* **1998**, *120*, 10234–10247.
(53) Osborne, E. M.; Ward, W. L.; Ruehle, M. Z.; DeRose, V. J. *Biochemistry* **2009**, *48*, 10654–10664.
(54) Chen, J. H.; Yajima, R.; Chadalavada, D. M.; Chase, E.; Bevilacqua, P. C.; Golden, B. L. *Biochemistry* **2010**, *49*, 6508–6518.
(55) Pontius, B. W.; Lott, W. B.; von Hippel, P. H. *Proc. Natl. Acad. Sci. U. S. A.* **1997**, *94*, 2290–2294.
(56) Rupert, P. B.; Ferre-D'Amare, A. R. *Nature* **2001**, *410*, 780–786.
(57) Nesbitt, S.; Hegg, L. A.; Fedor, M. J. *Chem. Biol.* **1997**, *4*, 619–630.
(58) Pinard, R.; Hampel, K. J.; Heckman, J. E.; Lambert, D.; Chan, P. A.; Major, F.; Burke, J. M. *EMBO J.* **2001**, *20*, 6434–6442.
(59) Park, H.; Lee, S. *J. Chem. Theory Comput.* **2006**, *2*, 858–862.
(60) Rhodes, M. M.; Réblová, K.; Šponer, J.; Walter, N. G. *Proc. Natl. Acad. Sci. U. S. A.* **2006**, *103*, 13380–13385.
(61) Ke, A. L.; Zhou, K. H.; Ding, F.; Cate, J. H. D.; Doudna, J. A. *Nature* **2004**, *429*, 201–205.
(62) Das, S. R.; Piccirilli, J. A. *Nat. Chem. Biol.* **2005**, *1*, 45–52.
(63) Nakano, S.; Chadalavada, D. M.; Bevilacqua, P. C. *Science* **2000**, *287*, 1493–1497.
(64) Nakano, S.; Proctor, D. J.; Bevilacqua, P. C. *Biochemistry* **2001**, *40*, 12022–12038.
(65) Wilson, T. J.; McLeod, A. C.; Lilley, D. M. J. *EMBO J.* **2007**, *26*, 2489–2500.
(66) Wilson, T. J.; Li, N. S.; Lu, J.; Frederiksen, J. K.; Piccirilli, J. A.; Lilley, D. M. J. *Proc. Natl. Acad. Sci. U. S. A.* **2010**, *107*, 11751–11756.
(67) Cochrane, J. C.; Lipchock, S. V.; Strobel, S. A. *Chem. Biol.* **2007**, *14*, 97–105.